transition temperature of near 90 K, the magnitude of the isotope shift is approximately the same as for $BaBi_{0.25}Pb_{0.75}O_3$, which has a T_c of only 11 K.

Measurements of the magnetic susceptibility of superconductors are sensitive to sample orientation in the magnetometer. Therefore, to verify that our data were not affected by sample orientation, that is, demagnetization effects, we conducted the following worst-case experiment. Magnetic data were collected for a pellet of $La_{1.85}Sr_{0.15}CuO_4$ when it was oriented perpendicular and parallel to the applied field. Although we did observe a small effect due to orientation on the measured susceptibility, it was small relative to the isotope shifts observed. Moreover, the diamagnetic onset does not depend on orientation. Therefore, we conclude that the isotope shifts are not produced by experimental artifacts.

Although it is possible to demonstrate the existence of an oxygen isotope effect, it is difficult to quantify the shift in T_c. This is because the diamagnetic transitions are relatively broad, and the magnitude of the shift is temperature-dependent. Furthermore, the samples are not isotopically pure, and it is not necessarily correct to assume a linear extrapolation to obtain the isotope effect for a sample with 100% ^{18}O. To measure the isotope shift quantitatively, one would need two samples, one with 100% ^{18}O and one with 100% ^{16}O, both showing identical Meissner effects and transition widths of at most 1 K.

Unless phonons are involved in the electron-pairing mechanism in these oxide superconductors, there is no reason for the superconducting transition temperatures to depend on the mass of oxygen. Therefore, the observation of an isotope effect confirms that phonons are involved in the electron-pairing mechanism in these oxide superconductors. It is significant that the magnitudes of the shifts in T_c when ^{18}O is substituted for ^{16}O are similar for all the samples. This is in contrast to what is predicted by BCS theory, assuming that Coulomb interactions do not vary substantially. It is possible that the Coulomb repulsion between electrons is larger in $YBa_2Cu_3O_7$ and $La_{1.85}Sr_{0.15}CuO_4$ than in $BaBi_{0.25}Pb_{0.75}O_3$, which would explain why smaller oxygen isotope effects are observed in the former samples. On the other hand, although phonons are definitely involved in the electron-pairing mechanism, there is a possibility of an additional interaction, several of which already have been proposed (*13–16*).

REFERENCES AND NOTES

1. J. Bardeen, L. N. Cooper, J. R. Schrieffer, *Phys. Rev.* **106**, 162 (1957).
2. A. W. Sleight, J. L. Gillson, P. E. Bierstedt, *Solid State Commun.* 17, 27 (1975).
3. J. G. Bednorz and K. A. Müller, *Z. Phys.* **B84**, 189 (1986).
4. M. K. Wu *et al.*, *Phys. Rev. Lett.* **58**, 908 (1987).
5. P. H. Hor *et al.*, *ibid.*, p. 911.
6. T. F. Faltens *et al.*, *ibid.* **59**, 915 (1987).
7. K. J. Leary *et al.*, *ibid.*, p. 1236.
8. G. F. Holland *et al.*, *ACS Symp. Ser.* **351**, 102 (1987).
9. S. W. Keller, K. J. Leary, A. M. Stacy, J. M. Michaels, *Mater. Lett.* **5**, 357 (1987).
10. S. W. Keller *et al.*, *ACS Symp. Ser.* **351**, 114 (1987).
11. B. Batlogg *et al.*, *Phys. Rev. Lett.* **58**, 2333 (1987).
12. L. C. Bourne *et al.*, *ibid.*, p. 2337.
13. V. L. Ginzburg, *Usp. Fiz. Nauk* **101**, 185 (1970) [*Sov. Phys. Usp.* **13**, 335 (1970)].
14. D. Allender, J. Bray, J. Bardeen, *Phys. Rev. B* 7, 1020 (1973).
15. D. Davis, H. Gutfreund, W. A. Little, *ibid.* **13**, 4766 (1976).
16. A. W. Sleight, *ACS Symp. Ser.* **351**, 2 (1987).

17. We thank A. Sleight for many useful discussions, and in particular for suggestions on how to prepare $BaBi_{0.25}Pb_{0.75}O_3$. We also thank Y. T. Lee, E. Hintsa, P. Chu, and A. Schmoltener for the $^{18}O_2$. This research was supported by the director, Office of Basic Energy Sciences, Materials Science Division, of the U.S. Department of Energy under contract DE-AC03-76SF00098. J.N.M. thanks the National Science Foundation for support under grant CBT-8552821.

19 August 1987; accepted 25 September 1987

Spectrophotometry of Pluto-Charon Mutual Events: Individual Spectra of Pluto and Charon

S. R. SAWYER, E. S. BARKER, A. L. COCHRAN, W. D. COCHRAN

Time-resolved spectra of the 3 March and 4 April 1987 mutual events of Pluto and its satellite Charon were obtained with spectral coverage from 5,500 to 10,000 angstroms with 25 angstrom spectral resolution. Since both events were total occultations of Charon by Pluto, spectra were obtained of the anti-Charon–facing hemisphere of Pluto, with no contribution from Charon during totality. On 4 April, a combined spectrum of Pluto and Charon immediately before first contact was also obtained. The spectrum of the Pluto-facing hemisphere of Charon was extracted by differencing the pre-event and totality spectra. The spectra were reduced to reflectances by ratioing them to spectra of solar analog stars. Charon has a featureless reflectance spectrum, with no evidence of methane absorption. Charon's reflectance appears neutral in color and corresponds to a geometric albedo of ~0.37 at 6000 angstroms. The Pluto reflectance spectrum displays methane absorption bands at 7300, 7900, 8400, 8600, and 8900 angstroms and is red in color, with a geometric albedo of ~0.56 at 6000 angstroms. The signal-to-noise ratios of the eclipse spectra were not high enough to unambiguously identify the weaker methane band at 6200 angstroms.

PLUTO AND ITS SATELLITE CHARON are the best example of a double planet in our solar system because of Charon's relatively large size compared to that of Pluto. Current estimates of the radii of the two bodies are 1210 and 590 km for Pluto and Charon, respectively (*1*). Thus, the presence of Charon accounts for nearly 20% of the total area of the Pluto-Charon system visible from Earth. However, the Pluto-Charon system is currently about 30 times farther from the sun than Earth. Consequently, the angular separation of the two bodies as seen from Earth is less than 1 arc sec, which is too small for any Earth-based instruments to resolve. Until recently, therefore, spectroscopic studies of Pluto and Charon have been limited to studies of the combined light from the two bodies.

The only features that have been identified in combined spectra of Pluto-Charon are a result of the presence of methane (CH_4), which displays characteristic absorption bands throughout the visible and near-infrared spectrum. Since the discovery of CH_4 on Pluto-Charon (*2*), researchers have attempted to model its distribution and state. Cruikshank *et al.* (*2*) interpreted their infrared photometry of Pluto-Charon as evidence for a CH_4 frost. Fink *et al.* (*3*) made the first high-quality observations of the CH_4 absorption bands in the region from 5,000 to 10,000 Å. They modeled the observed spectrum by assuming that the absorptions occurred within a CH_4 atmosphere and found that the weak bands (6200, 7900, and 8400 Å) displayed a linear relation between band depth and CH_4 abundance for the band depths present in the observed spectra. However, models of the strong bands (7300 and 8900 Å) displayed little variation in band depth with CH_4 abundance for the observed band depths. Fink *et al.* (*3*) argued that the saturation of the strong bands demonstrated the presence of a CH_4 atmosphere on Pluto (Charon's spectrum was ignored in their models) since

Department of Astronomy and McDonald Observatory, The University of Texas at Austin, Austin, TX 78712.

Fig. 1. Relative reflectances of Pluto (top) and Charon (bottom), normalized to 1.0 to 6000 Å in the Pluto spectrum. The feature near 7600 Å is a result of imperfect cancellation of the atmospheric O_2 A band. There are no visible features in the Charon spectrum with the proper location or shape to be CH_4 absorption.

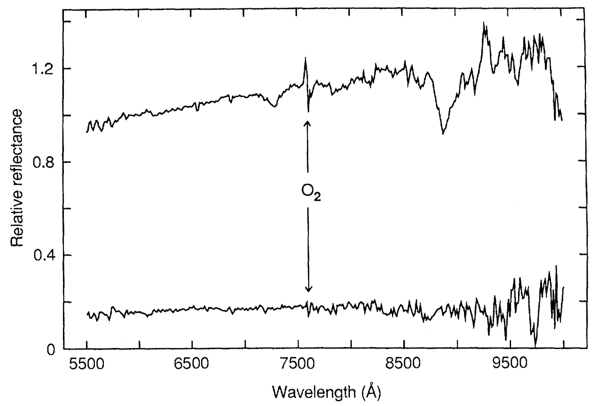

absorption in solid or liquid CH_4 is linear with abundance. If the observed CH_4 absorption does arise from gas, then a global surface temperature for Pluto of 55 to 58 K is required to maintain the volatile atmosphere (*4, 5*). Since the solar equilibrium temperature is 43 K, this temperature difference would have to be investigated. Possible explanations include a greenhouse effect or internal heat source on Pluto or a low thermal emissivity (ability to radiate away thermal energy) for solid CH_4 (*4*).

Further clues about the state of the CH_4 on Pluto-Charon are provided by the rotation of Pluto. Pluto has a rotational period of about 6.4 days, which is also the period of revolution of Charon around Pluto since the two bodies are tidally locked. During this time, Pluto-Charon varies in brightness by about 0.3 magnitude (about 30%) as a result of albedo (surface reflectivity) variations on the surfaces of the bodies. Buie and Fink (*6*) obtained time-resolved spectra of Pluto-Charon over a full rotational period and reported variation in the depths of the CH_4 bands. They concluded that the bands arose from a surface CH_4 frost whose uneven longitudinal distribution on the surface of Pluto was also responsible for the observed rotational light curve. They proposed that the apparent saturation of the strong bands could be explained by multiple scattering effects within a frost, which would deepen the weak bands relative to the strong bands. In their models, Buie and Fink (*6*) assumed that Charon has no CH_4 and has a reddish spectrum similar in albedo to that of Pluto. Sawyer (*5*) also obtained time-resolved spectra of the Pluto-Charon system. He observed no significant variability in the CH_4 bands and concluded that the CH_4 absorption arose primarily from uniformly distributed atmospheric CH_4 gas, with a small contribution from the surface frost. For his models, Sawyer (*5*) assumed that Charon has a reddish continuum reflectance with a slope similar to that of Pluto, a slightly lower average albedo than Pluto, and no CH_4. As this overview suggests, the source of the CH_4 absorptions on Pluto-Charon is disputed, and the inability to measure the contribution of Charon to the combined light from the system has exacerbated the problem. Charon's color, albedo, and CH_4 abundance (if any) have been left as free parameters in models, although Charon is probably unable to maintain a significant atmospheric or surface abundance of CH_4 (*7*).

The opportunity to study Pluto and Charon as separate bodies would constitute a major breakthrough in the struggle to understand not only the current state of this double planet, but also its history and origin. Specific knowledge of Charon's reflectance spectrum would provide accurate constraints for model calculations of its contribution to the total light from the system. These calculations would make it possible to use previous combined Pluto-Charon observations to study the surface and atmosphere of Pluto, which would help resolve whether Pluto has a significant atmosphere. In addition, the reflectance of Charon can place important constraints on the origin of the Pluto-Charon system (*7*). Because of its small size and low mass, Charon is unlikely to have melted and differentiated early in its history. Thus, study of the surface composition of Charon could provide clues to the composition of the material in which the Pluto-Charon system formed. This information could help distinguish whether Pluto-Charon formed directly from the solar nebula or from a protoplanetary nebula. The latter would be the case if they formed as satellites of another planet, such as Neptune or Uranus (*7*).

In early 1985, Binzel *et al.* (*8*) made the first observations of a series of Pluto-Charon mutual events. In a superior event, Pluto occults Charon (primary passes in front of satellite); in an inferior event, Charon transits Pluto (satellite passes in front of primary). These events are occurring as the plane of Charon's orbit around Pluto sweeps across Earth, and they should occur about every 3.2 days (alternately superior and inferior) for the next several years. The series of mutual events occurs only once every 124 years. By timing these events researchers are able to determine the orbital parameters, radii, and densities of these bodies far more accurately than could be achieved by previous methods. In addition, the occultations provide the first opportunity to obtain spectra of the two bodies individually. By obtaining a spectrum immediately before a superior event and a spectrum during totality (when Charon is completely occulted by Pluto), one obtains a spectrum of the anti-Charon–facing hemisphere of Pluto directly, and, by differencing the two, a spectrum of the Pluto-facing hemisphere of Charon. Charon's surface reflectance characteristics can then be directly inferred. This method requires a total occultation and provides information about the average reflectances of only one hemisphere of each body. Inferior events provide information about the opposite hemispheres. However, Charon does not completely occult Pluto, making interpretation of observations of these events more difficult. More generally, the difference between the pre-event and event spectra for any event provides an average spectrum for the obscured area. If a sufficient number of events are observed at varying geometries, it is possible to map the surface reflectances of both bodies. The mapping resolution depends on the time required to obtain individual spectra compared to the time scale for the events, and it must necessarily be crude, although better than a hemisphere scale. We report here the results of two nights of observing total superior events. For the purposes of obtaining a basic characterization of the surface reflectance of Charon, only pre-event and totality spectra are considered here.

The 3 March and 4 April 1987 Pluto-Charon mutual events (*9*) were observed with the McDonald Observatory 2.1-m Struve reflector. We used the electronic spectrograph 2 with an RCA SID52501 front side–illuminated charge-coupled device (CCD). The spectrograph has been described in detail by Tull *et al.* (*10*) and has recently been modified for use with a CCD. The CCD is a two-dimensional detector consisting of a 512 by 320 array of pixels. The spectrograph disperses light along the 512-pixel axis, producing 100 spatially resolved spectra of a strip of sky about 3 arc min in width (*11*). Since the object image is typically only a few arc seconds across, simultaneous observations of the sky on both sides of the object are obtained. The particular grating-detector combination we used covered the spectral range of 5,500 to 10,000 Å with 25 Å spectral resolution.

To correct for terrestrial atmospheric O_2

and H_2O absorption features present throughout the spectral region, we observed flux standard stars several times each at different airmasses during each night (*12*). Flux standard stars are stars with known energy fluxes that are used to calibrate the absolute flux being received for each object observed. Observing a star at a number of different airmasses (as it rises, reaches maximum elevation, and sets) allows one to calculate the extinction (absorption of light by Earth's atmosphere) as a function of airmass for each of the 512 wavelength bandpasses. Separate solutions for several stars can be averaged to improve accuracy. The extinction solution can then be used to correct for the effects of atmospheric extinction in other observations from the same night. We also observed several solar analog stars (stars with spectra as similar as possible to the spectrum of the sun) on each night. These stars were chosen from Hardorp's (*13*) list of solar analog candidates. Table 1 contains the observation logs for the two nights. Each entry represents an average of three or more exposures.

In the early evening of 3 March the sky was marginally suitable for our observations, but a minimal set of flux standard, extinction, and solar analog star observations were barely completed before the sky clouded over at 0700 UT. After a brief rain, the sky cleared up at 1045 UT, which was after the start of the event, so Pluto was observed for the balance of the night. No

Table 1. Log of observations.

Object	Start time (UT)	Exposure (seconds)	Airmass
	3 March 1987		
η Hya*	0322	1.6	1.22
Hyades 64†	0341	30.0	1.37
Hyades 63†	0349	30.0	1.42
θ Crt*	0432	2.4	2.08
η Hya*	0450	1.6	1.13
θ Crt*	0503	2.4	1.83
35 Leo†	0530	3.0	1.03
θ Crt*	0541	2.4	1.58
η Hya*	0656	1.6	1.29
Pluto‡	1053	5400.0	1.19
	4 April 1987		
Hyades 64†	0230	100.0	1.77
θ Crt*	0254	4.4	1.80
η Hya*	0309	2.4	1.13
θ Crt*	0401	4.0	1.47
109 Vir*	0513	1.6	1.94
θ Crt*	0525	3.3	1.31
η Hya*	0536	3.0	1.49
Pluto§	0608	3600.0	1.38
109 Vir*	0727	1.6	1.22
θ Crt*	0739	3.6	1.53
θ Crt*	0848	4.2	2.06
Pluto‡	0915	2880.0	1.18
16 Cyg B†	1129	22.5	1.18

*Flux and extinction star. †Solar analog star. ‡Event totality. §Pre-event.

pre-event spectra of Pluto-Charon were obtained. Since a high airmass observation of η Hya was not obtained, only θ Crt was used as a flux and extinction standard. In addition, the rain caused a substantial change in the humidity, rendering the extinction observations made earlier in the evening suspect. The night of 4 April was clear throughout, but the humidity was variable. Consequently, the extinction solutions calculated for the three standard stars were in poor agreement. The most reasonable-looking solution resulted from 109 Vir, which is also currently very near Pluto in the sky as seen from Earth. Therefore, we used only 109 Vir as a flux and extinction standard.

We subtracted a dark exposure of equal length from each of our program exposures in order to remove any contribution to the spectra that was intrinsic to the CCD detector. We then corrected the exposures for inherent pixel-to-pixel sensitivity differences by using flat field exposures of a lamp projected onto the dome ceiling. The reflected lamp light evenly illuminated the spectrograph entrance slit, so that variations in detected light across the slit could be interpreted as sensitivity differences. Since the CCD is a two-dimensional detector, one can obtain a simultaneous exposure of a program object in the center of the slit and of the nighttime sky at either end of the slit. The contribution of light from the nighttime sky was subtracted and the spectra were collapsed to one dimension by means of the optimal extraction algorithm of Horne (*14*). A wavelength scale was calculated from exposures of argon and neon hollow cathode spectra. The pixel-by-pixel extinction correction and flux calibration of the data were then performed.

Each Pluto-Charon exposure was reduced independently up to this point, when they were averaged according to whether they were pre-event or totality spectra. Four individual pre-event exposures of 15 minutes each and four totality exposures of 12 minutes each were taken to produce the entries in Table 1. Simultaneous broadband photometry of the occultations was performed by Binzel (*15*) on the McDonald 2.7-m telescope. Our definitions of pre-event and totality times were taken from Binzel's photometric record and confirmed by our own observations. We ratioed these averaged spectra to solar analog spectra to remove solar features and residual instrumental response features not removed by the flux calibration. Observations of solar analog stars were preferred to the use of actual solar spectra obtained from another source in order to match the instrumental resolution of the Pluto-Charon observations. We chose 35 Leo for 3 March since it was the closest match to the Pluto airmass; 16 Cyg B was chosen for 4 April for the same reason. At this point, the pre-event and totality spectra were differenced for the 4 April event. The relative reflectances of the two bodies, scaled to 1.0 at 6000 Å in the Pluto spectrum, are shown in Fig. 1.

Geometric albedos were calculated for the two bodies at 6000 Å in the manner described by Sawyer (*5*). The radii adopted for these calculations were 1210 km for Pluto and 590 km for Charon (*1*). A 5% decrease in the adopted radius of a body would correspond to a 10% increase in geometric albedo. The calculated geometric albedo for Pluto at 6000 Å was ~0.56 for the 4 April data. A value of ~0.53 was calculated for the 3 March data. These values are consistent with each other and allow an estimate of ~0.03 for the uncertainty in the measurement. The calculated geometric albedo for Charon at 6000 Å was ~0.37. The signal-to-noise ratio for the Pluto spectrum ranges from nearly 200 at the blue end to about 20 at the red end, whereas the signal-to-noise ratio for the Charon spectrum ranges from about 25 to 3. Although the Charon spectrum does show some structure between 8000 and 9000 Å, the positions of these features are not correlated with the positions of the strong CH_4 bands. Inspection of the Charon spectrum at 7300 and 8900 Å revealed no traces of the strong bands within the noise. Its spectrum is apparently featureless and neutral in color. The anti-Charon–facing hemisphere of Pluto displays identifiable CH_4 bands at 7300, 7900, 8400, 8600, and 8900 Å. The slope of the spectrum indicates that this hemisphere of Pluto is considerably redder than the Pluto-facing hemisphere of Charon. An upper limit on the strength of CH_4 absorption in the Charon spectrum can be obtained by considering the equivalent widths of the CH_4 bands (*16*). The equivalent widths of the strongest bands in the Pluto reflectance spectrum, at 7300 and 8900 Å, are 10.6 and 47.9 Å, respectively. An estimate of the root-mean-square error in an equivalent width measurement (ϵ_W) can be made by using the method of Jenkins *et al.* (*17*). An upper limit on the equivalent width of an undetected feature can then be set at $\sim 2\epsilon_W$. For the 7300 and 8900-Å bands in the spectrum of Charon, the upper limits are 5 and 22 Å, respectively. Therefore, the CH_4 on Charon is depleted by at least 50% compared to Pluto.

The apparent depletion of CH_4 on Charon is consistent with calculations that show that it should have quickly lost any surface CH_4, although it may have a significant amount of CH_4 in clathrates within the body (*7*). Pluto, however, should have maintained a significant surface abundance of CH_4. The redness of Pluto with respect to Charon probably arises from long-chain molecular products of the photolysis of CH_4 by solar ultraviolet insolation (7). By the same reasoning, the neutral color of Charon is further evidence of the absence of CH_4 on the surface of that body. Charon's geometric albedo falls within the range of the geometric albedos of the major Uranian satellites (0.18 to ~0.5), all of which are known to have water ice surfaces (18). The possible detection of H_2O ice on Charon by Marcialis *et al.* (19) therefore provides a reasonable explanation of its geometric albedo. The surface reflectance properties of Pluto and Charon are controlled by ices and cannot be classified to an asteroid taxonomy, which characterizes surface mineralogy.

REFERENCES AND NOTES

1. D. J. Tholen, *Int. Astron. Union Circ. 4403* (1987).
2. D. P. Cruikshank, C. B. Pilcher, D. Morrison, *Science* **194**, 835 (1976).
3. U. Fink, B. A. Smith, D. C. Benner, J. R. Johnson, H. J. Reitsema, *Icarus* **44**, 62 (1980).
4. L. Trafton and S. A. Stern, *Astrophys. J.* **267**, 872 (1983).
5. S. R. Sawyer, thesis, University of Texas at Austin (1986).
6. M. W. Buie and U. Fink, *Icarus* **70**, 483 (1987).
7. L. Trafton, S. A. Stern, R. Gladstone, paper presented at the Symposium on the Origin and Evolution of Planetary and Satellite Atmospheres, Tucson, AZ, 10 to 14 March 1987.
8. R. P. Binzel, D. J. Tholen, E. F. Tedesco, B. J. Buratti, R. M. Nelson, *Science* **228**, 1193 (1985).
9. D. J. Tholen, M. W. Buie, C. E. Swift, *Astron. J.* **93**, 244 (1987).
10. R. G. Tull, S. S. Vogt, P. W. Kelton, *Soc. Photo-Optical Instrum. Eng.* **172**, 90 (1979).
11. Because the entrance aperture of the spectrograph only projects onto about one-third of the width of the CCD, 100 spectra are produced (instead of 320).
12. Airmass is a term used to describe the thickness of atmosphere that light passes through before reaching the observer. It is defined to be one when the object is at the zenith (directly overhead) and increases as an object gets closer to the horizon. The airmass is approximately equal to the secant of the angle between the zenith and the line of sight to the object.
13. J. Hardorp, *Astron. Astrophys.* **63**, 383 (1978).
14. K. Horne, *Publ. Astron. Soc. Pac.* **98**, 609 (1986).
15. R. P. Binzel, personal communication.
16. Equivalent width is a measure of the amount of light that is absorbed in a spectral feature. It represents the width (in angstroms) of a feature with the same amount of absorption that has zero intensity across its entire width.
17. E. B. Jenkins *et al.*, *Astrophys. J.* **181**, L122 (1973).
18. D. P. Cruikshank and R. H. Brown, in *Satellites*, J. A. Burns and M. S. Matthews, Eds. (Univ. of Arizona Press, Tucson, 1986), pp. 836–873.
19. R. L. Marcialis, G. H. Rieke, L. A. Lebofsky, paper presented at the Symposium on the Origin and Evolution of Planetary and Satellite Atmospheres, Tucson, AZ, 10 to 14 March 1987.

20. Supported by NASA grant NGR 44-012-152.

8 June 1987; accepted 24 September 1987

Genetic Ablation: Targeted Expression of a Toxin Gene Causes Microphthalmia in Transgenic Mice

MARTIN L. BREITMAN, SUSAN CLAPOFF, JANET ROSSANT, LAP-CHEE TSUI, L. MICHAEL GLODE, IAN H. MAXWELL, ALAN BERNSTEIN

Lineage-specific regulatory elements can be used to direct expression of a variety of genes to specific tissues in transgenic mice. If the hybrid constructs contain a gene encoding a cytotoxic gene product, then genetic ablation of a specific cell lineage can be achieved. We have generated six transgenic mice by introducing into fertilized eggs the mouse γ2-crystallin promoter fused to the coding region of the diphtheria toxin A-chain gene. Three of these mice and all the transgenic offspring analyzed were microphthalmic. The lenses of these mice displayed considerable heterogeneity: some were almost normal morphologically but reduced in size, whereas others were grossly aberrant and deficient in nuclear fiber cells. These studies indicate that programmed ablation of specific cell types can be stably transmitted through the germ line.

CONSIDERABLE PROGRESS HAS BEEN made in the understanding of the origins and interrelations of cell lineages during growth and development in invertebrates such as *Caenorhabditis elegans* and *Drosophila* (1). Lineage development in mammals is not as well understood, however, because of the indeterminate or stochastic nature of cell commitment during embryogenesis. Several experimental approaches have been applied to this problem, including microinjection of histochemical tracers, direct visualization of developing embryos, photoablation, and the generation of mosaic and chimeric animals (2). Recently, new genetic approaches to lineage analysis have been developed. These include the use of in situ hybridization to recognize cells of different genotypes in mouse chimeras or mosaics (3), the exploitation of retrovirus vectors as random insertional tags within both the hematopoietic system (4) and the developing mouse embryo (5), and the utilization of the bacterial *lacZ* gene as an in situ marker for visualizing lineage-specific gene expression (6) and cell-lineage relations (7). Here, we demonstrate that targeted expression of the gene for the A chain of diphtheria toxin (DT-A) in transgenic animals results in the death of a specific cell type during development, a method that we have termed "genetic ablation." Palmiter *et al.* (8) have independently described a similar approach to effect the ablation of cells within the pancreas.

To demonstrate the feasibility of this approach, we used the mouse γ2-crystallin promoter to target expression of the DT-A gene to the mouse eye lens. The DT-A gene encodes an adenosine diphosphate (ADP) ribosyltransferase that catalyzes the ADP-ribosylation of elongation factor 2, resulting in the inhibition of protein synthesis and subsequent cell death (9). As little as one molecule per cell of the DT-A chain is estimated to be cytotoxic (10).

The γ2-crystallin promoter was chosen to drive expression of the DT-A gene for the following reasons. (i) This promoter can direct expression of a *lacZ* reporter gene exclusively to the lens fiber cells of transgenic mice (6). (ii) Ablation of cells within the lens would be expected to result in a readily discernible phenotype (see below). (iii) The relation between crystallin gene expression and lens cell differentiation is well characterized. (iv) Many developmental mutants that affect the lens have been described, which provides a basis for interpreting lens phenotypes caused by ablation events. (v) Developmental aberrations within the lens are nonlethal, and thus would not complicate initial efforts to evaluate the potential of genetic ablation.

The lens consists predominantly of two cell types: undifferentiated epithelial cells, which make up the anterior surface layer, and terminally differentiated fiber cells, which constitute the major body of the lens. Because synthesis of γ-crystallins, as well as the activity of the mouse γ2 promoter in transgenic mice, is restricted to terminally differentiated fiber cells of the lens nucleus (6, 11), it was anticipated that expression of the DT-A gene from the mouse γ2 promoter in transgenic mice would result in a lens

M. L. Breitman, J. Rossant, A. Bernstein, Mount Sinai Hospital Research Institute, 600 University Avenue, Toronto, Ontario, Canada M5G 1X5, and Department of Medical Genetics, University of Toronto, Toronto, Ontario, Canada M5S 1A8.
S. Clapoff, Mount Sinai Hospital Research Institute, 600 University Avenue, Toronto, Ontario, Canada M5G 1X5.
L.-C. Tsui, Department of Genetics, Hospital for Sick Children, 555 University Avenue, Toronto, Ontario, Canada M5G 1X8, and Department of Medical Genetics, University of Toronto, Toronto, Ontario, Canada M5S 1A8.
L. M. Glode and I. H. Maxwell, Division of Medical Oncology, University of Colorado Health Sciences Center, Denver, CO 80262.